Land Surface Initialization Using an Offline CLM3 Simulation with the GSWP-2 Forcing Dataset and Its Impact on CAM3 Simulations of the Boreal Summer Climate*

JEE-HOON JEONG

School of Earth and Environmental Sciences, Seoul National University, Seoul, Korea, and Department of Earth Sciences, University of Gothenburg, Gothenburg, Sweden

CHANG-HOI HO

School of Earth and Environmental Sciences, Seoul National University, Seoul, Korea

DELIANG CHEN

Department of Earth Sciences, University of Gothenburg, Gothenburg, Sweden

TAE-WON PARK

School of Earth and Environmental Sciences, Seoul National University, Seoul, Korea

(Manuscript received 18 June 2007, in final form 16 May 2008)

ABSTRACT

The impacts of initialized land surface conditions on the monthly prediction were investigated using ensemble simulations from the Community Atmosphere Model version 3 (CAM3). The land surface initialization was based on an offline calculation of Community Land Model version 3 driven by observation-based meteorological forcings from the Global Soil Wetness Project 2 (GSWP2). A simple but effective correction method was applied to the GSWP2 forcings prior to the offline calculation to reduce the discrepancies between the observation-forced land surface conditions and the modeling system, which can cause climate drift and initial shock problems. The climatological mean of GSWP2 forcings was adjusted to that of the target model (CAM3), while the monthly anomalies were scaled to the model statistics and high-frequency synoptic variabilities were included.

Ensemble hindcast experiments with and without land surface initialization were conducted for the boreal summer (May–September), for 1983–95. The initialization process is shown to prevent climate drift and to transfer the atmospheric anomalies to the land surface memory. Statistical analyses of the simulation results reveal that the land surface initialization increased the externally forced variance over most continental regions, which is translated to enhanced potential predictability, particularly for regions with strong land–atmosphere coupling.

1. Introduction

Land surface processes have a significant impact on the climate system through the exchange of energy and moisture with the overlying atmosphere. Due to their longer persistence relative to the chaotic behavior of the atmosphere (Vinnikov et al. 1996; Liu and Avissar 1999; Wu and Dickinson 2004), it is widely recognized that the slowly varying land surface conditions—soil moisture, subsurface temperature, and snow cover—modulate the overlying atmosphere in direct and/or indirect ways. In fact, many land–atmosphere coupled general circulation model (GCM) studies emphasize the usefulness of land surface conditions for extended and seasonal predictions (e.g., Dirmeyer 2000; Koster and Suarez 2003; Koster et al. 2004a,b; Kanae et al. 2006; Conil et al. 2007). In particular, the land–atmo-

* The Centre of Earth System Science at the University of Gothenburg (Tellus) Contribution Number 15.

Corresponding author address: Chang-Hoi Ho, Climate Physics Laboratory, School of Earth and Environmental Sciences, Seoul National University, Seoul 151-742, Korea.
E-mail: hoch@cpl.snu.ac.kr

DOI: 10.1175/2008JHM941.1

sphere interaction accounts for much of the atmospheric variability over continental regions, a feature that can be potentially translated into predictability enhancement, while the influence of the ocean is mostly confined to the tropical and subtropical regions (Koster et al. 2000; Koster and Suarez 2003).

Although the importance of land surface initialization is widely recognized, there are still several difficulties to be resolved before it can be applied practically to extended and seasonal prediction. The most important requirement is a realistic estimate of land surface conditions that can be used as the initial conditions in land–atmosphere coupled GCM simulations. However, both the temporal resolution and spatial coverage of direct measurements of land surface variables are too limited to be directly applicable to GCM simulations (Entin et al. 2000; Robock et al. 2000). Several attempts have been made to retrieve soil moisture using satellite remote sensing, but generally the results are only applicable to the thin upper soil layer where atmospheric signals are dominant on short time scales (Wagner et al. 1999). Using the linear lead–lag relationship between the surface and root-zone soil moisture shown in offline land surface model (LSM) simulations, Hirabayashi et al. (2003) suggested an algorithm to retrieve root-zone soil moisture values from the Tropical Rainfall Measuring Mission (TRMM) based surface soil moisture retrieval by Oki et al. (2000). However, the TRMM-based surface soil moisture retrieval has a deficiency over vegetated regions and is only really available for subtropical latitudes. Calvet et al. (1998) suggested an alternative method for retrieving root-zone soil moisture from surface soil moisture using an assimilation technique, but this approach makes intensive use of datasets at both high spatial and temporal resolutions.

As a result, sophisticated LSMs are widely used to indirectly estimate land surface conditions. Driven by accurate and relatively abundant atmospheric observations, an LSM can estimate physically consistent land surface variables such as soil moisture and subsurface temperature, which are used as the initial conditions in a land–atmosphere coupled GCM simulation. Previous studies have investigated this approach for the land surface initialization in GCM simulations and generally reported a modest but significant increase in predictability from incorporating realistic land surface conditions (e.g., Dirmeyer 2000; Koster and Suarez 2003; Koster et al. 2004a). Land surface estimates are highly dependent on the selected LSM and atmospheric forcings, so many attempts have also been made to reduce uncertainties by using multi-LSM-based calculations with high quality atmospheric forcings that combine direct observations with reanalysis (International GEWEX Project Office 2002; Dirmeyer et al. 2004).

Another consideration is that the signals memorized by land surface conditions should be effectively translated into the climate model system in a consistent manner. To this end, a precise dynamical–physical treatment of the GCM–LSM to resolve realistic land–atmosphere interaction is essential; moreover, the compatibility of the land surface estimates with the target model should be ensured. Because most GCMs still have a considerable bias with regard to the observations, the land surface conditions estimated by observational forcings are inevitably biased relative to the GCM climatology. Such a discrepancy is known to lead to an improper depiction of the climatic regime that determines the characteristics of the land–atmosphere interaction (Mahanama and Koster 2005) and to the so-called climate drift problem—initialized land surface states rapidly drift toward a chosen AGCM's own climatology at an early stage of simulation (Dirmeyer 2001). Both problems eventually diminish the simulated land–atmosphere interaction. Thus, Dirmeyer et al. (2004) and Koster et al. (2004a) have pointed out the necessity of postprocessing land surface estimates before they are applied in a GCM simulation.

The objective of the present study is to develop an appropriate land surface initialization method that addresses the above-mentioned considerations. The primary strategy is to develop a bias correction and scaling process for the observed meteorological forcings, which drive an offline LSM simulation for land surface initialization. Since this approach employs a high quality meteorological dataset from the Global Soil Wetness Project 2 (GSWP2: International GEWEX Project Office 2002), it is expected to ensure that the initial land surface estimates are both accurate and compatible with the GCM, and so avoid the climate drift problem. Ensemble simulations from the Community Atmospheric Model version 3 (CAM3) are performed both with and without the estimated land surface conditions as initial conditions, and the impact of the land surface initialization on the GCM's predictability is evaluated.

This paper is organized as follows. Section 2 describes the experimental design, including the models; the land surface initialization processes; and the ensemble simulations performed. Section 3 then presents the results of the experiments; the effectiveness of the bias correction and the predictability changes due to the land surface initialization are presented based on several statistical evaluation techniques. A summary and discussion are presented in section 4.

TABLE 1. Description of the GSWP2 atmospheric forcing data.

Variable	Data source
Temperature	Monthly CRU data hybridized with the 3-hourly NCEP–DOE reanalysis near-surface air temperature at 2 m
Wind speed	NCEP–DOE reanalysis wind speed at 10 m
Specific humidity	NCEP–DOE reanalysis near-surface specific humidity at 2 m
Incident short- and longwave radiation	Surface radiation budget data produced at NASA Langley Research Center
Precipitation	Hybridized GPCC, CRU gauges, and NCEP–DOE reanalysis

2. Experimental design

a. Model

CAM3, the fifth generation atmospheric GCM developed by the National Center for Atmospheric Research (NCAR), is used. The horizontal and vertical resolutions of this model are spectral T42 (approximately 2.875° × 2.875°) and 26 hybrid-sigma levels, respectively. The most up-to-date dynamical treatments and physical parameterization schemes are incorporated into CAM3, and details are documented in Collins et al. (2004, 2006).

The Community Land Model version 3 (CLM3; Bonan et al. 2002; Oleson et al. 2004) is the land surface parameterization incorporated into CAM3. Coupled with CAM3 of T42 horizontal resolution, the global land surface comprises 3799 grid points, each of which are represented as a nested subgrid composed of five primary subgrid land cover types: glacier, lake, wetland, urban, and vegetated. These subgrids further consist of 10 soil columns for the calculation of the soil temperature and soil water contents and 5 snow columns for the treatment of snow depth. The vegetated subgrid is composed of up to 4 different plant functional types from a total 15 types.

The present study uses the land–atmosphere coupled CAM3–CLM3 (hereafter CAM3) for ensemble simulation and an offline version of CLM3 (without direct interaction with CAM3) for land surface initialization.

b. Initialization procedures

The "proxy" land surface conditions estimated from the offline calculation of the LSM were used as the initial land surface conditions for the ensemble simulations. While the LSM continuously exchanges energy and moisture with the overlying atmosphere in the coupled mode, in offline-mode LSM evolves under the prescribed atmospheric states and fluxes. Here, we used the offline version of CLM3 and the atmospheric forcings provided by GSWP2 for land surface initialization.

The aim of GSWP2 is to measure global land surface estimates in agreement with multi-LSM offline calculations (Dirmeyer et al. 2006). The GSWP2 forcings are created from various combinations of global observations and model-based reanalysis products to give global coverage and to resolve high-frequency temporal variations (Zhao and Dirmeyer 2003; see Table 1). GSWP2 products include global 3-hourly surface air temperature, wind speed, specific humidity, incident short- and longwave radiation, and precipitation at 1° × 1° resolution. In addition to these time-varying atmospheric forcings, the GSWP2 provides the fixed surface parameters that are used for the boundary conditions of the LSM (such as soil type, elevation, vegetation type, and wilting levels) to allow direct intercomparison among the offline results of LSMs. In the present study, however, we only used the time-varying forcings from the GSWP2; the specified boundary parameters were those that were originally incorporated in CAM3.

Even using such high quality atmospheric forcings to produce the initial land surface conditions does not ensure that the AGCM accurately simulates the land–atmosphere interaction. The main reasons are as follows. First, there are still too many uncertainties in current LSMs to resolve complex land surface processes. This might be the primary reason why there is a considerable degree of error in simulated LSM results. Second, even if accurate land surface conditions were estimated by perfect LSM and forcings data, the inconsistency between the LSM estimations and the AGCM may cause a climate drift problem in a land surface-initialized AGCM simulation. Despite great progress in the development of AGCMs in recent decades, most AGCMs continue to have large biases with respect to observations (Gates et al. 1999). Consequently, there could be a large climatological discrepancy between LSM estimates forced by observational data and those simulated by the AGCM–LSM coupled system. When LSM estimates forced by observations are used without correcting the initial conditions in an ensemble simulation, the biased land surface conditions tend to drift toward the AGCM–CLM coupled system's individual climate state (Dirmeyer 2000, 2001; Koster and Suarez 2003). Such climate drift can quickly remove the

"memory" contained in land surface conditions, or it can act as an initial shock. Thus, compatibility between the land surface estimates and the target AGCM must be ensured before the land–atmosphere interaction can be simulated appropriately.

The left panels in Fig. 1 display the climatological differences between the observations (GSWP2 forcings) and a CAM3 Atmospheric Model Intercomparison Project (AMIP; Gates et al. 1999) type simulation for precipitation, air temperature, and wind speed at the lowest level of the atmosphere, and net surface radiation flux over land areas. These differences demonstrate the problem of using CAM3 to drive an LSM, particularly for surface fluxes. The most notable features are warm and dry biases over northern Eurasia, Canada, East Asia, India, the Middle East, and the Sahara Desert, and relatively cold and wet biases over America, South America, and the coastal region around the Mediterranean Sea (Figs. 1a and 1c). Overall, there is a dry bias over the major precipitation zones and a wet bias over many arid or desert regions; these are the well-known common deficiencies of existing GCMs reported in the AMIP results (Gates et al. 1999). These biases appear to be highly correlated with the strong biases of the net incident radiation (Fig. 1b), which dominates the surface energy balances as well as local evapotranspiration and the subsequent hydrological cycle. In the model, the surface wind is generally weaker than that obtained from observations over most of the global continents except the Tibetan region (Fig. 1d). The right panels in Fig. 1 represent the results of the bias correction that was applied in the present study, which will be discussed in section 3a below.

Undoubtedly, if an AGCM could be greatly improved so that it is unbiased with respect to the observations, then the observation-forced LSM estimates could be used directly as the initial land surface conditions and there would be no climate drift or initial shock problem. However, the performance of existing AGCMs does not satisfy this prerequisite. As a compromise between the AGCM's deficiency and our aim of realistically initializing land surface conditions, we attempted to adjust the observed "forcings" to match the target AGCM's climatology. Assuming that the AGCM's capability to produce atmospheric anomalies from given anomalous boundary conditions (e.g., SST and land surface) was reliable, we adjusted the climatology of GSWP2 forcings to the target GCM's climatology and rescaled the anomalies based on the local statistics of the model and the observations. Thus, it was expected that the mean bias correction would prevent the climate drift problem, while the rescaled anomalies would yield realistic anomalies for land surface states and provide a longer memory for the atmosphere.

The bias correction and anomaly scaling procedure were as follows. Values of 3-hourly atmospheric temperature, wind speed, and specific humidity at the near-surface region were modified:

$$(X_F)_{Y,M,D,H} = (\overline{X}_{\mathrm{AMIP}})_{Y,M} + (X'_{\mathrm{GSWP}})_{Y,M}\frac{\sigma[(X'_{\mathrm{AMIP}})_{Y,M}]}{\sigma[(X'_{GSWP})_{Y,M}]} + (X^{*}_{\mathrm{GSWP}})_{Y,M,D,H}, \quad (1)$$

where X denotes any parameter; subscript F, forcing; Y, year; M, month; D, day; H, hour; superscript $'$, monthly anomaly; and *, high-frequency variability. First, the monthly anomaly from the GSWP2 13-yr mean, X'_{GSWP}, was extracted and scaled using the monthly based ratio of two interannual standard deviations ($\sigma[(X'_{\mathrm{AMIP}})_{Y,M}]/\sigma[(X'_{\mathrm{GSWP}})_{Y,M}]$), the latter obtained from GSWP2 and an AMIP-type GCM simulation (a control experiment, which is referred to as AMIP in Table 2). Second, the scaled monthly anomalies were added to the monthly climatology of the control simulation ($\overline{X}_{\mathrm{AMIP}}$). Then, the part representing the high-frequency variability (X^{*}_{GSWP}), which was obtained by determining the difference between the raw data (X_{GSWP}) and their centered 64-point (8 days) moving average values, was added in consideration of the diurnal cycle and synoptic variability. The result obtained (X_F) should ensure consistency between the monthly anomalies of GSWP data and the climatological mean of the target model CAM3.

For the adjustments of the radiation flux and precipitation, a different method [Eq. (2)] was applied due to the characteristics of these variables:

$$(X_F)_{Y,M,D,H} = (X_{\mathrm{GSWP}})_{Y,M,D,H}\frac{(\overline{X}_{\mathrm{AMIP}})_M}{(\overline{X}_{\mathrm{GSWP}})_M}. \quad (2)$$

The precipitation in a certain grid box is a positive definite quantity with frequent zeroes; therefore, a bias correction method based on Eq. (1) could produce negative values. Moreover, very small $\sigma(X'_{\mathrm{GSWP}})$ values appeared in high-latitude continental regions, making it difficult to apply Eq. (1). The radiation fluxes also suffer from a similar problem due to their sharp diurnal variations. Therefore, we tried to reduce the mean bias using different kinds of scaling factors based on the ratio of the monthly seasonal cycle of the CAM3 climate to that of GSWP2, rather than using bias subtraction and anomaly scaling as per Eq. (1). Finally, the mean bias between the GSWP2 dataset and the model is reduced by the multiplicative scaling factor

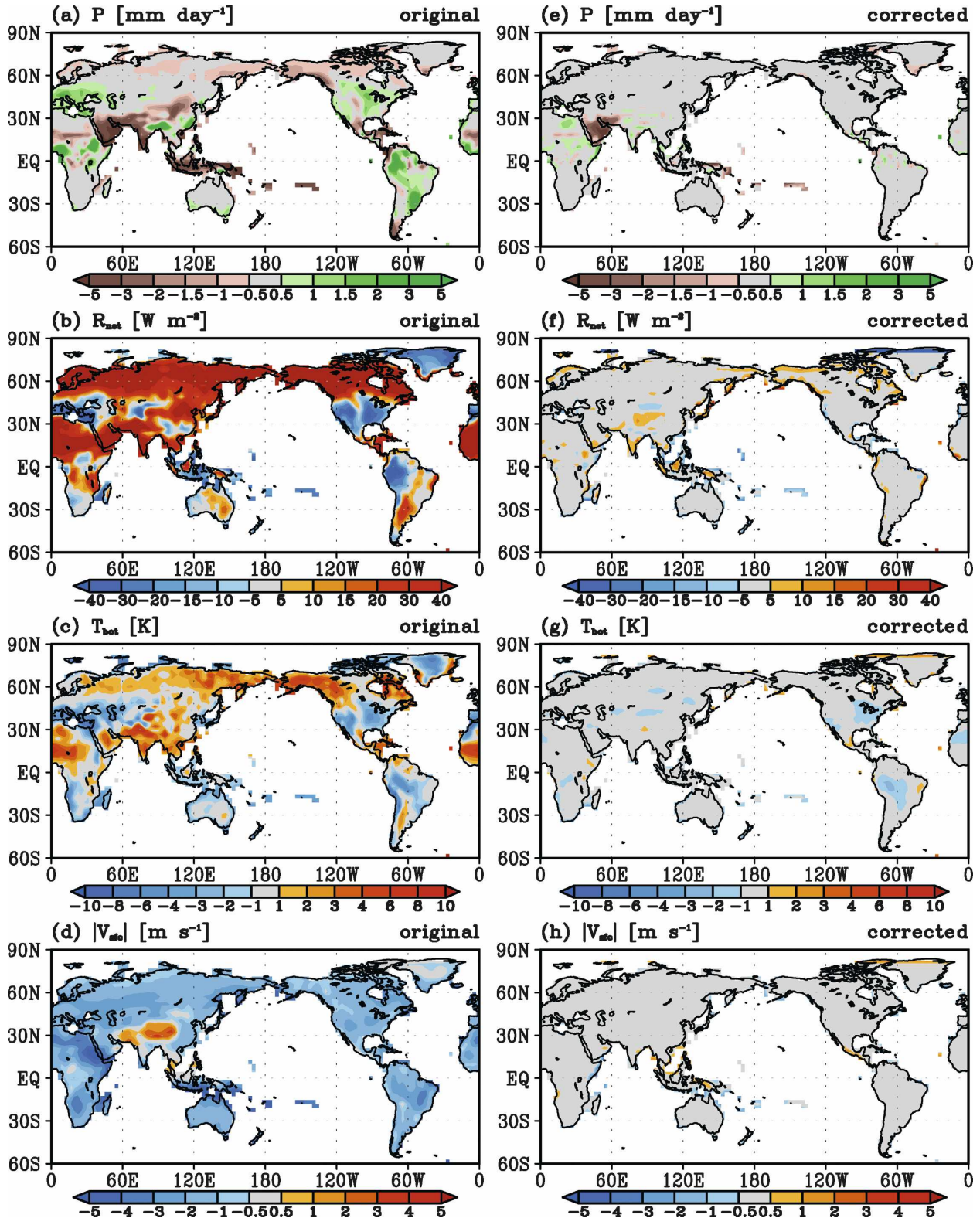

FIG. 1. Climatological difference between observations (GSWP2) and CAM3 AMIP simulations (AMIP) averaged from May to September for (a), (e) precipitation (P), (b), (f) net surface radiation (R_{net}), (c), (g) surface air temperature (T_{sfc}), and (d), (h) surface wind speed ($|V_{sfc}|$), for (left) original GSWP2 forcings and (right) bias-corrected forcings.

TABLE 2. Summary of experiments performed.

Model	Expt	Forcings/SSTs	Land surface initial conditions	Experiment period
CLM3 (offline)	L_NOC	GSWP2 before correction	Spun up for 13 yr	1983–95
	L_COR	GSWP2 after correction		
CAM3	AMIP	Observed SST	Initialized from AMIP-type simulations from 1950	1979–2002
	ALIC		Initialized from L_COR	May–Sep 1983–95
	ALIC_CLIM		Initialized from climatology of L_COR	May–Sep 1986–95
	ALIC_NOC		Initialized from L_NOC (no correction)	May–Sep 1993–95

$(\overline{X}_{\mathrm{AMIP}})_M/(\overline{X}_{\mathrm{GSWP}})_M$ to avoid the above-mentioned problems. In the present study, offline LSM and ensemble AGCM–LSM experiments were performed at T42 resolution, so the GSWP2 data were horizontally interpolated to T42 resolution before the bias correction process.

Dirmeyer et al. (2004) suggested a similar method of "renormalization" to reduce the initialization shock caused by applying precalculated soil wetness estimates as the initial conditions for other climate models. Using a similar approach, Koster et al. (2004a) utilized "standard normal deviates" of the offline-calculated land surface estimates. Both of these are postprocessing methods, which can be done after offline LSM calculation. One important limitation of such methods is that all of the land surface conditions would be corrected or normalized separately. For example, 15 variables in an initial condition of CLM3, such as soil moisture, soil temperature, vegetation–ground temperature, snow states (depth and age), canopy–ground-water, and so on, would be corrected one variable at a time. However, some of them are physically dependent on each other, so such corrections may introduce physical inconsistencies between variables. As an alternative, we attempted to suppress the possibility of climate drift in CAM3 simulations at the stage of preparing atmospheric forcing data, that is, prior to performing the offline LSM simulation. It is possible that our approach also produces some physical inconsistencies in the LSM forcing, because each of the forcing variables is adjusted separately. However, inconsistencies will presumably be small because only the monthly anomalies are corrected, while the synoptic- and shorter-scale variabilities are preserved. Consequently, the present methodology enables physically consistent land surface variables to be estimated using a single run and eliminates the need for further corrections. The results of the bias correction, and the impact on the LSM simulation, will be presented in section 3a.

One thing to note is that GSWP2's basic data period is 10 yr from 1986 to 1995, and the driving data before 1986 (July 1983–December 1985) were created with limited data for spinup simulation of the project. Therefore, there is a difference in the forcing data between the spinup and basic periods. During the spinup period, the University of East Anglia's Climate Research Unit (CRU) data are used for precipitation instead of Global Precipitation Climatology Center (GPCC) data due to the unavailability of the GPCC data [in both periods, CRU and GPCC data are combined with data from the National Centers for Environmental Prediction–Department of Energy (NCEP–DOE) reanalysis]. Also SRB data are not available during the spinup period, so the averages of 10 (January–October) or 9 (November–December) yr hybridized with NCEP–DOE data were used for the spinup period. In the present study, model simulations were performed for both the spinup and basic periods, so as to use as many samples as possible. However, only the results for the basic period were used to perform analyses with respect to observational values (e.g., R^{*2} statistics, to be described in section 3c).

c. Experiments performed

First, two sets of the offline LSM calculation—the L_NOC (offline LSM, no correction) and the L_COR (offline LSM, correction)—were performed. The L_NOC was driven by the original GSWP2 forcings without bias correction, as described in section 2b, while the L_COR was driven by the corrected forcings, as described in section 2b. To obtain reliable estimates of temperature and moisture throughout the model soil layers, both L_NOC and L_COR were spun up for 13 yr. By cycling the 13-yr GSWP2 forcings (or corrected GSWP2 forcings) twice, each offline LSM calculation was integrated for 26 yr and results from the second cycle of integration were utilized. The L_NOC was used as a control offline LSM simulation to check the effects of bias correction by comparison with the L_COR simulation. The initial land surface conditions on the first day of each month were taken from L_NOC and L_COR and then saved and used for the subsequent AGCM ensemble simulations.

Four sets of AGCM ensemble simulations were performed to examine the impact of the initialized land surface conditions on monthly prediction in CAM3. The first experiment is referred to as AMIP and was a

parallel 10-member ensemble AMIP-type simulation coupled with a freely evolving CLM3 (without land surface initialization) with the prescribed observed sea surface temperature (RSST; Reynolds and Smith 1994) for the period 1979–2002. One initial land surface condition and 10 initial atmospheric conditions were chosen from a 50-yr integration of CAM3 with climatological SSTs, then parallel AMIP-type runs were integrated from 1950 to 1979 to yield land initial conditions of the "AMIP" experiment. Thus, the land surface conditions in the AMIP experiment were consistent with the concurrent SST distribution.

The second experiment is ALIC (i.e., an AGCM experiment with land surface initial conditions), a land-initialized ensemble experiment of CAM3, which was performed to assess the impact of land initialization by comparison with the AMIP. For boreal summer (May–September) from 1983 to 1995 (total 65 months), 1-month integrations with 10 ensemble members were simulated with the initial land surface conditions calculated in the L_COR simulation. The SST used was always the same as that in the AMIP, and the atmospheric initial conditions of the 10 ensemble members were obtained from the AMIP simulation. Thus, the ALIC experiment was identical to the AMIP experiment, except for the land surface initial conditions. In all there were 650 samples from the AMIP and ALIC simulations, which allowed the impact of initial land surface conditions to be examined with sufficient statistical significance.

The third experiment, ALIC_NOC, was identical to ALIC except it used initial land surface conditions from L_NOC (i.e., the land surface conditions were uncorrected). Comparing ALIC and ALIC_NOC allowed the impact of the bias correction to be examined.

The fourth experiment, ALIC_CLIM, was also identical to ALIC but used the L_COR climatology (10-yr averages of the land surface variables) as land surface initial conditions; that is, the interannual variations in land surface condition were removed. This experiment was used to examine the impact of interannual variations in land surface conditions on prediction by comparison with ALIC.

The CLM3 and CAM3 experiments performed in the present study are briefly summarized in Table 2.

3. Results

a. The impact of bias correction

First, the impact of the bias correction on the offline CLM3 simulation was examined by comparing experiments L_NOC and L_COR. Figure 2 depicts the climatological mean bias of the L_NOC (left panels) and the L_COR (right panels) with respect to the AMIP results of the target AGCM (CAM3). Evaporation, soil moisture in the upper soil layer (0–0.2 m) and the deep soil layer (0.2–1 m), and sensible heat flux at the surface are shown. In L_NOC, the simulated evaporation and soil moisture in the upper soil layer (Figs. 2a–c) generally represented a dry bias in the major tropical precipitation zones and a wet bias in many extratropical dry regions. These are closely connected with the excessive sensible heat over the northern extratropics and desert regions and deficient sensible heat over tropical regions (Fig. 2d). Furthermore, in the deep soil layer, a negative bias of soil moisture is found over northern Eurasia and America, a phenomenon largely due to the biases in precipitation and radiation forcings (see Figs. 1a and 1b).

With bias correction (L_COR), most of the mean differences were reduced considerably (Figs. 2e and 2f). In particular, much of the excessive evaporation and sensible heat in the extratropics disappeared. Still, some positive soil moisture and related negative evaporation bias is found over tropical regions (Figs. 2e–g), which might to be due to the precipitation bias that remains in spite of the correction process. But most of those biases are found over the maritime continents and coastal regions where the fraction of the land surface is relatively low. Also, soil moisture biases remain over high, latitudinal regions (especially in the deep soil layer where the adjustment time is quite long), but it appears that these are not closely related to the surface fluxes. Thus, the L_COR results did show that the corrections could suppress climate drift and initial shock problems over the extratropics.

Next, we examined the impact of bias correction on the CAM3 simulations. Figure 3 represents the differences in soil moisture (for the top 50 cm) between the first and second weeks of May in 1993–95 for ALIC_NOC (left panels) and ALIC (right panels). Before correction (ALIC_NOC), in all three of the example cases, the first weeks show drier soils over the middle of Africa and Southeast Asia, but wetter soils over mid–northern America. This clearly represents a strong drift from the initial soil moisture fields. The results for ALIC do not show any such bias pattern and exhibit interannual variations in the soil moisture field over the regions where strong biases are found in ALIC_NOC. Figure 4 shows the time evolution of soil moisture averaged over the eastern United States (32.5°–37.5°N, 102.5–97.5°W) and mid-China (32.5°–37.5°N, 105°–115°E), where prominent wet and dry biases in ALIC_NOC are found. This clearly demonstrates the climate drift in ALIC_NOC and also the impact of bias correction on ALIC; while the ALIC_NOC simulations rap-

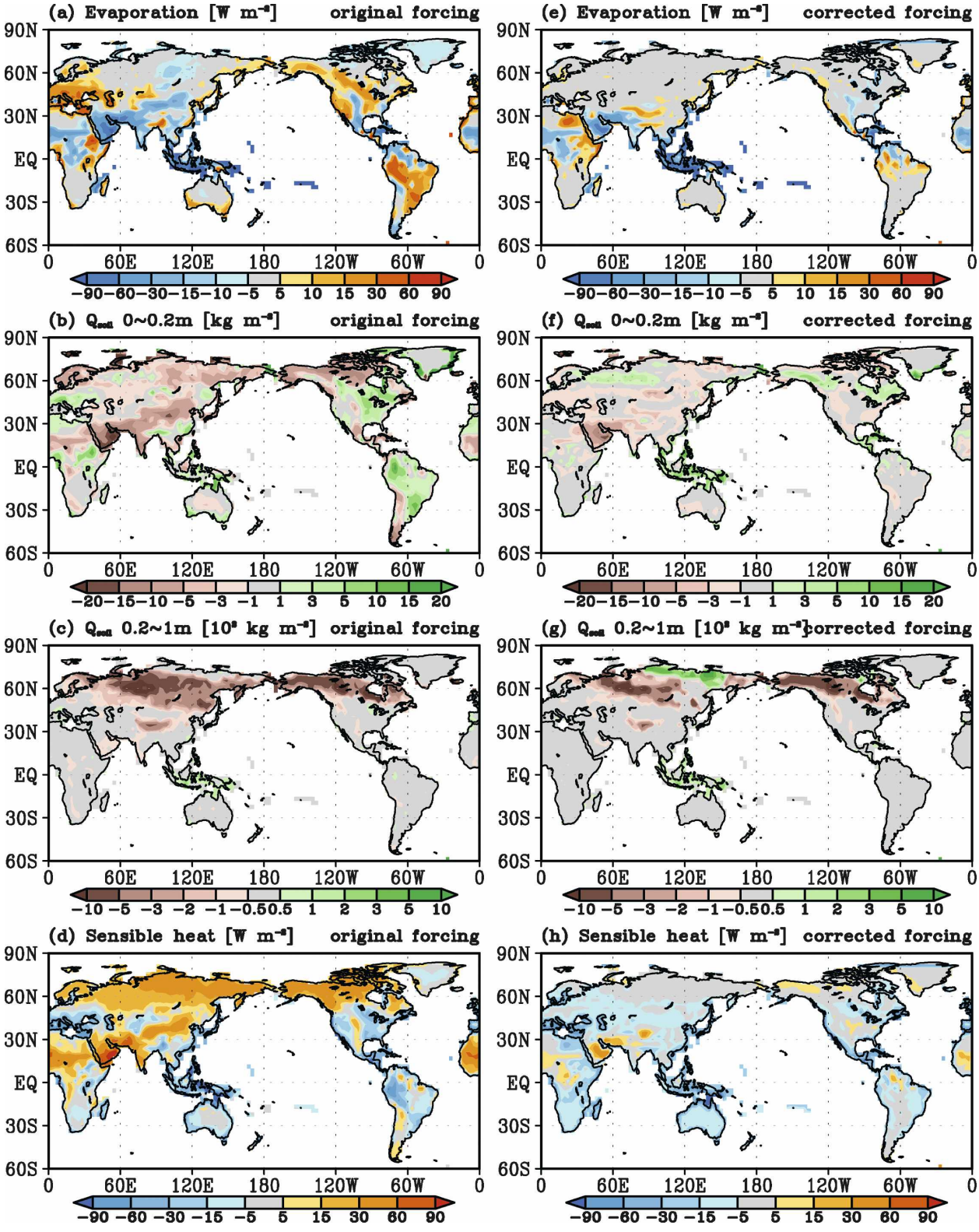

FIG. 2. Climatological difference between offline simulations of CLM3 and CAM3 (active CLM3 coupled) AMIP simulations averaged from May to September, for (a), (e) evaporation, soil moisture in (b), (f) upper (0~0.2 m) and (c), (g) lower (0.2~1 m) layers, and (d), (h) sensible heat for results (left) forced by original GSWP2 forcings and (right) by bias-corrected forcings.

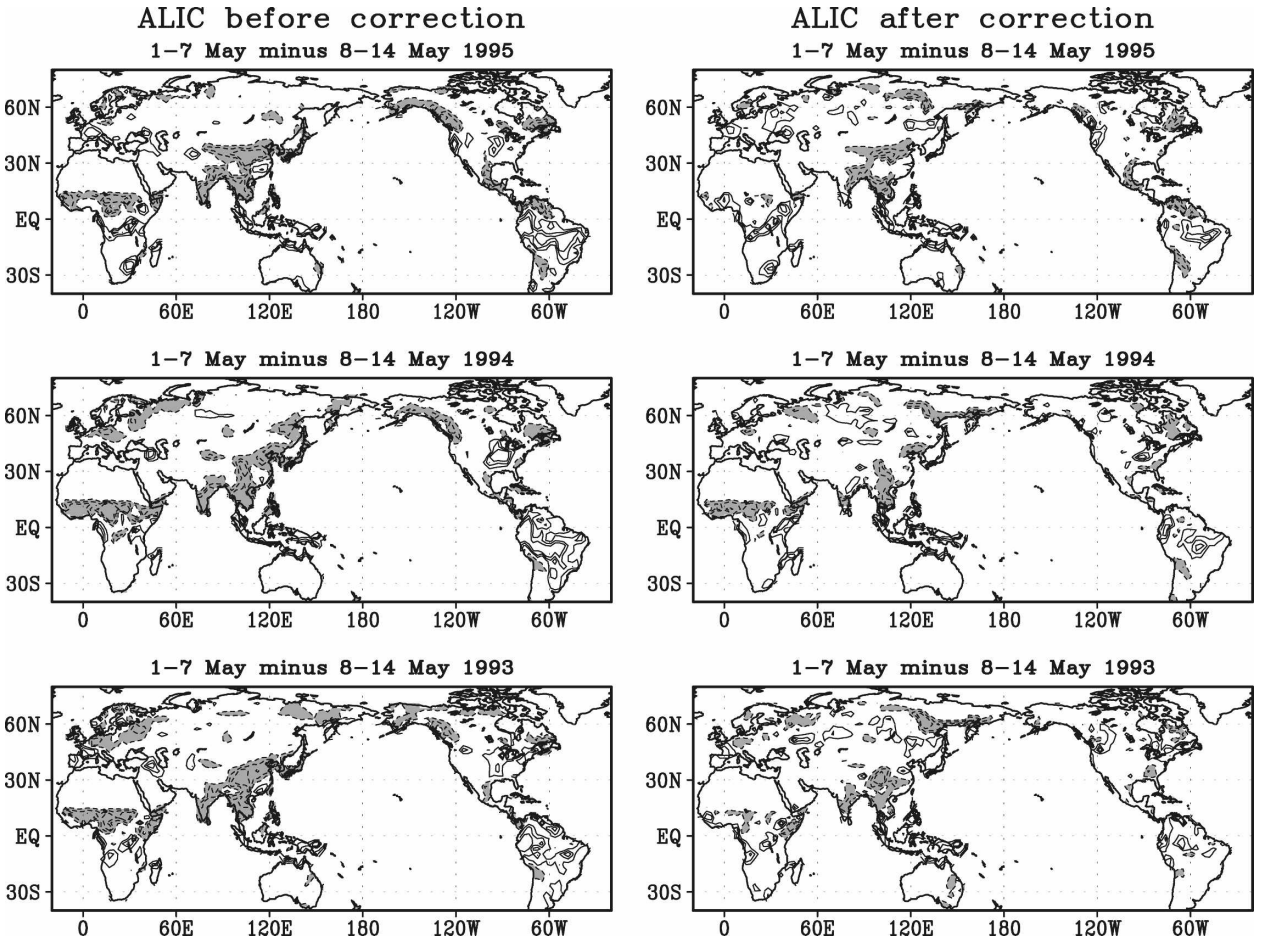

FIG. 3. Difference between soil moisture in top 50 cm averaged in first and second week of May in 1993–95, for (left) ALIC_NOC (without a correction process) and (right) ALIC: (top) 1995, (middle) 1994, and (bottom) 1993. Solid and dashed lines indicate positive and negative contours with 1% intervals (values less than −1% are shaded).

idly drift toward the AMIP values (i.e., reference states of CAM3) in the early stages of the simulation (the first 2–3 weeks), the ALIC simulations evolve around the AMIP values. A strong climate drift is found in other land surface and near-surface variables as well, and also in other months/years of the ALIC_NOC experiment (figure not shown). With such a bias, prediction results would be expected to deteriorate in the first few weeks, and monthly forecasts could also be affected.

Because bias correction was shown to be effective in removing climate drift, the impacts of the initialized land surface conditions on prediction skill were examined, as discussed in the next section.

b. The impacts on potential and practical predictability

To evaluate the impacts of land surface initialization, the results of the ALIC and the AMIP simulations were examined using several objective statistics: signal-to-noise ratio (Shukla 1981; Rowell 1998; Kang and Shukla 2006), idealized explained variance R^2 (Koster et al. 2004a), and signed explained variance R^{*2} (Dirmeyer et al. 2006). The impacts of land surface initialization on climate prediction were examined by comparing the results of the ALIC and the AMIP.

The signal-to-noise ratio is defined as being the ratio between the variance that is externally forced by boundary conditions (namely SST and land surface conditions) and the variance that is generated internally by the chaotic atmosphere. The basic premise behind this estimate is that differences among the ensemble members result from the internal dynamics of the atmosphere, whereas the ensemble mean represents the atmospheric response to slowly varying external forcings such as SSTs and land surface conditions. As suggested by Rowell (1998), the total variance of an ensemble simulation (σ^2_{tot}) can be decomposed into exter-

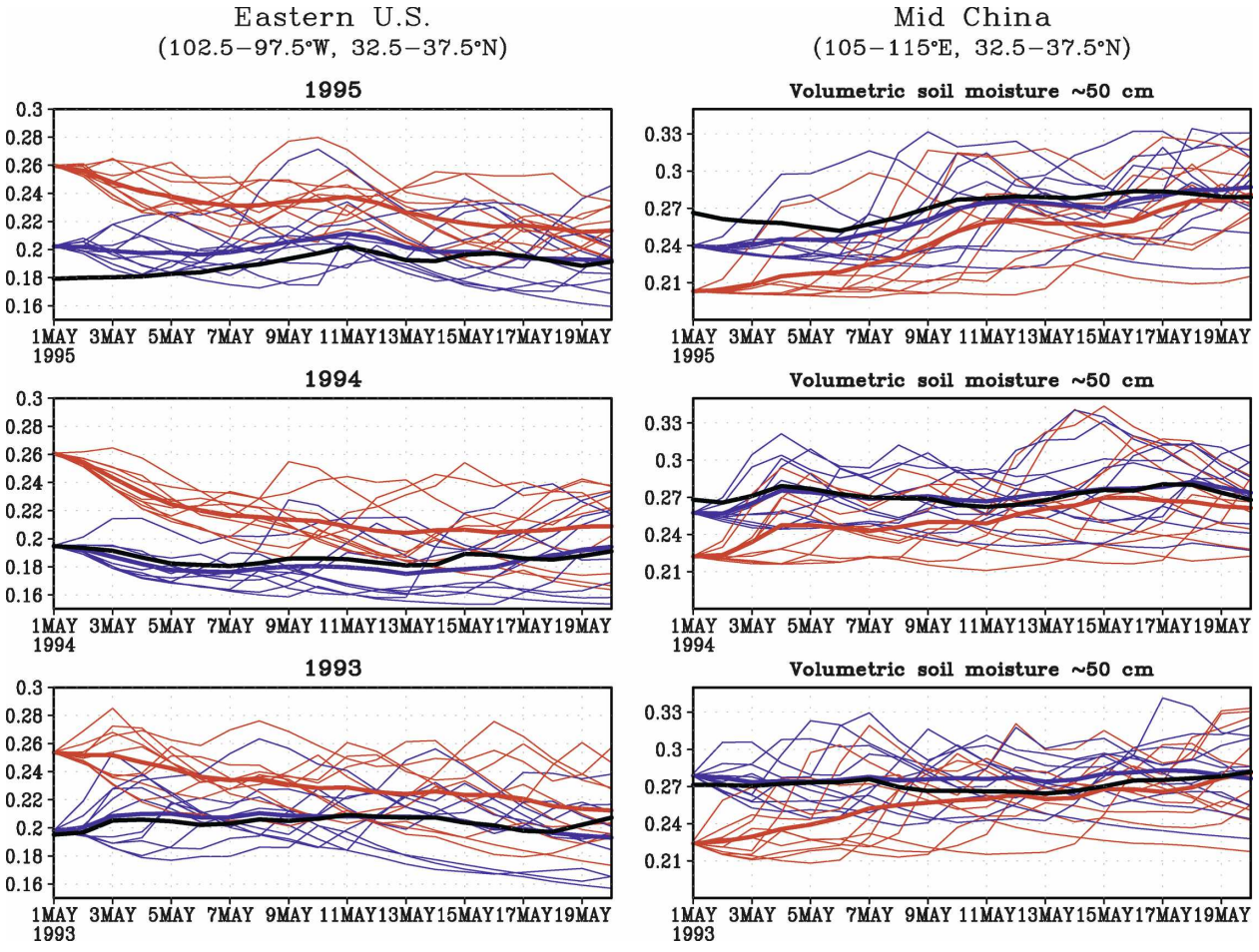

FIG. 4. Time evolution of volumetric soil moisture for ALIC (blue line) and ALIC_NOC (red lines) in top ~50 cm for 1–20 May in (top) 1995, (middle) 1994, and (bottom) 1993. Thick colored line indicate the ensemble mean value. Thick black line indicates the value for the AMIP ensemble mean. (left) The eastern United States (32.5°–37.5°N, 102.5°–97.5°W) and (right) middle China (32.5°–37.5°N, 105°–115°E).

nal signal (σ^2_{ext}) and internal noise (σ^2_{int}) variances. The variances σ^2_{ext} and σ^2_{int} are expressed as follows:

$$\sigma^2_{\text{ext}} = \sigma^2_{\text{ensm}} - \frac{1}{n}\sigma^2_{\text{int}} \quad \text{and} \quad \sigma^2_{\text{int}} = \frac{1}{N(n-1)} \sum_{i=1}^{N} \sum_{j=1}^{n} (x_{ij} - \overline{x_i})^2 \tag{3}$$

$$\sigma^2_{\text{ensm}} = \frac{1}{N-1} \sum_{i=1}^{N} (\overline{x_i} - \overline{\overline{x}})^2, \tag{4}$$

where i is the number of ensemble forecasts performed ($N = 65$), j is the number of ensemble members ($n = 10$), ensm is for ensemble, $\overline{x_i}$ the ensemble mean, and $\overline{\overline{x}}$ the climatological mean. By definition, the ratio between σ^2_{ext} and σ^2_{int} indicates the signal-to-noise ratio of the modeling system: it signifies how effectively the prescribed SSTs and initialized land surface conditions determine the atmospheric anomalies.

For the precipitation and surface air temperature simulations (hereafter referred to as P and T_{sfc}, respectively), the signal-to-noise ratio of ALIC and its difference from the AMIP (impacts of land surface initialization) are shown in Fig. 5. As shown in Figs. 5a and 5b, large external signals are mostly observed over tropical oceans where the direct response of the atmosphere to the prescribed SSTs is strong, while the internal noise is greater than the external signal over most of the extratropical continental regions. However, over some continental regions the externally forced variance exceeds the internal variance (i.e., the signal-to-noise ratio is greater than 1). For P forecasts, relatively large values are obtained over subtropical latitudes such as southern Asia, the Indian subcontinent, middle Africa, the central United States, and South America (Fig. 5a). The

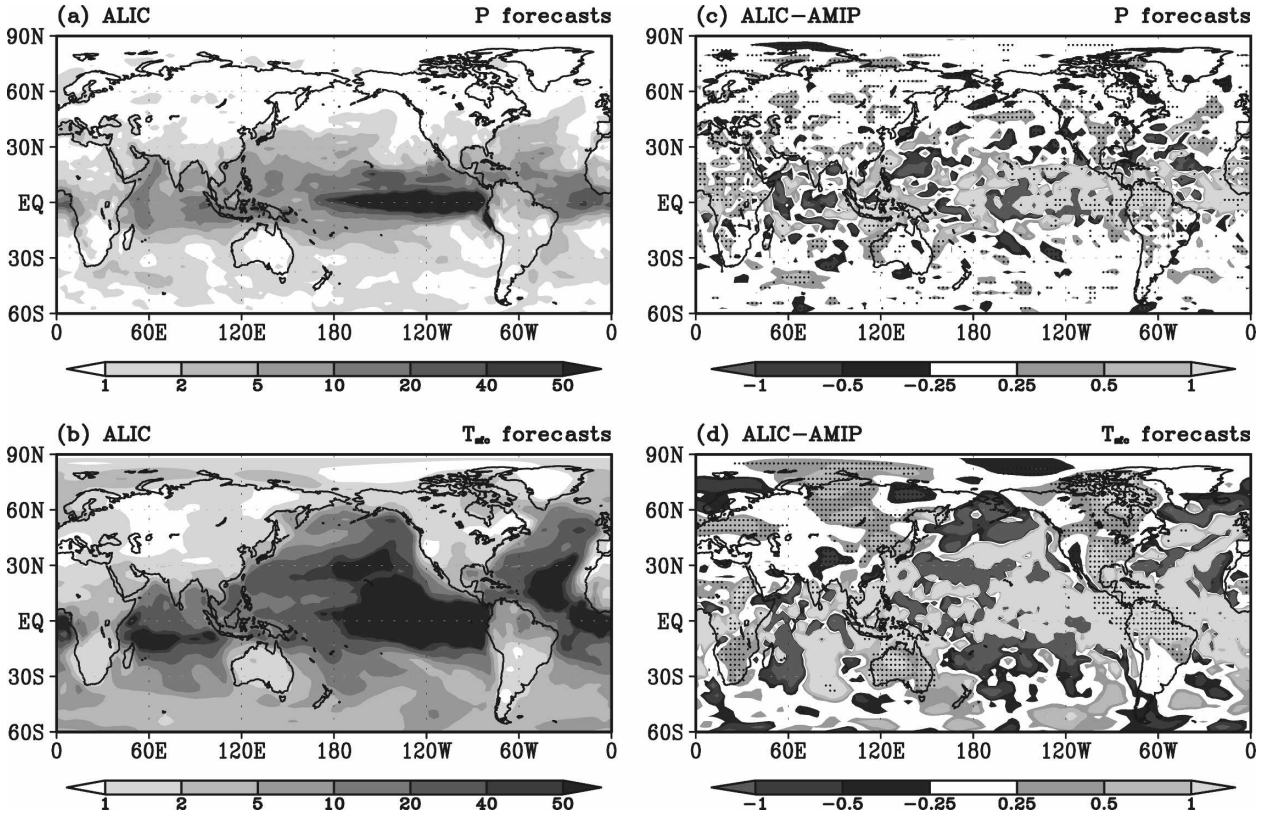

FIG. 5. (left) Signal-to-noise ratio of ALIC and (right) its difference with respect to that of the AMIP simulation, for (a), (c) precipitation and (b), (d) surface air temperature. In (c) and (d), regions with differences >20% of the signal-to-noise ratio of AMIP are indicated by small dots.

signal-to-noise ratio of T_{sfc} exhibits a similar distribution; however, its magnitude greatly exceeds that of precipitation (Fig. 5b). The increase in the external variance by the land surface conditions is also observed over many parts of continental regions (Figs. 5c and 5d). The increase in the external variance is greater and more spatially coherent in the T_{sfc} forecasts than in the P forecasts, but the P forecasts still exhibit positive values (an increase in external variance) over most of the continental regions. Considering that the remote influences of SST represent a large portion of the external signals over land areas, the differences between the ALIC and the AMIP simulations (Figs. 5c and 5d) demonstrate a considerable increase in signal resulting from using initialized land surface conditions. Compared with the changes over land areas, the impact of land surface initialization over the oceans is very small.

It is noted that the signal-to-noise ratio values were dependent on the precipitation regime, as shown in Table 3. Here, the signal-to-noise ratio values are categorized into humid, intermediate, and dry precipitation regions, which were determined from the climatological mean precipitation in May–September. For both P and T_{sfc} forecasts, the increase in the signal-to-noise ratio is greatest over humid regions. The T_{sfc} forecasts show a larger increase than does the P forecasts, and a considerable increase is still found over intermediate and dry regions. As the percentage increases with respect to AMIP values, the P forecasts in humid and intermediate regions represent similar increases of

TABLE 3. Spatially averaged signal-to-noise ratio. Humid, intermediate, and dry regions are where the climatological mean precipitation of AMIP averaged from May to September is >5, 2–5, and <2 mm day^{-1}, respectively. Values in parentheses in the last column are the percentage difference with respect to AMIP values.

	Region	ALIC	AMIP	Difference
Precipitation	Humid	4.38	3.83	0.55 (14)
	Intermediate	1.84	1.61	0.23 (14)
	Dry	1.20	1.11	0.09 (8)
	Global	1.86	1.66	0.20 (12)
Surface air temperature	Humid	6.74	5.57	1.17 (21)
	Intermediate	2.93	2.44	0.49 (20)
	Dry	1.86	1.54	0.32 (21)
	Global	2.39	1.97	0.42 (21)

about 14%, which was higher than the 8% found in dry region. For the T_{sfc} forecasts, all three regions showed similar increases of about 21%.

The signal-to-noise ratio results indicate that the initialized land surface conditions induce additional external variance over land areas. However, further evaluation was necessary to determine whether the increased external variance actually increased the predictability. To this end, the R^2 statistics (Koster et al. 2004a) of the ALIC and the AMIP experiments were calculated and compared, to evaluate the predictability change resulting from land surface initialization. The R^2 statistics are based on the conventional r^2 (square of correlation) statistics from linear least-square curve fitting, but are slightly modified so they can be used to estimate the consistency among the ensemble forecasts. In brief, R^2 was computed as follows. Assuming the first ensemble member as an observation, its correlation coefficient (r) with the ensemble mean of the remaining nine ensemble members was computed through linear regression of the 65 observation–forecast pairs, and then the r^2 values were estimated in the global domain. In the above calculation, r^2 values were set to zero if a certain point had a negative value of r, considering it as a sampling problem. The process was repeated with the remaining nine ensemble members, and the average of the resulting 10 r^2 arrays yielded the R^2 statistics of the modeling system. Thus, the resulting R^2 values represent the upper limit of the modeling system forecasts, which is interpreted as the variance that is explained by the prescribed SSTs and the initialized land surface conditions. Note that the R^2 statistic only represents "idealized" explained variance, is not a measure of the actual predictability with respect to the observations. In an ensemble AGCM simulation, the evolution of each ensemble member is very sensitive to the initial atmospheric conditions because of atmospheric chaos. However, the four AGCM ensemble simulations from the present study used initial atmospheric conditions taken from a parallel AMIP-type ensemble simulation without including any observed atmospheric field. Thus, here we are first attempting to examine "idealized" skill, which is not limited by errors in the initial atmospheric conditions. The "practical" predictability increase achieved by land surface initial conditions (i.e., with respect to observed values) is discussed in the next section.

Figure 6 shows the R^2 for the P and T_{sfc} forecasts in the ALIC and AMIP simulations; the differences between the two experiments represent the increase in the predictability associated with the land surface initialization. For the P forecasts, the relatively high r^2 values are mostly observed within subtropical latitudes (30°S–30°N) adjacent to tropical oceans (Figs. 6a and 6b). A large increase in potential predictability is noticed over middle Africa, the Tibetan Plateau, mid- to western Russia, and northern South America (Fig. 6c). The regions of high R^2 values for the T_{sfc} forecasts mostly overlapped with those of the P forecasts, but exhibited larger magnitudes and wider areal extents. In particular, relatively high R^2 values were found over high-latitude regions such as northern Eurasia and Canada, as well as over Australia, where there was no significant improvement in the P forecasts. By again categorizing the R^2 results into mean precipitation regimes (Table 4), it is observed that the regional dependence of the impacts of land initialization is similar to that of the signal-to-noise ratio: large R^2 values and an increase due to the land initialization are found over humid and intermediate regions. For the global average, the R^2 values of the P and T_{sfc} forecasts are about 10% (from 7% in dry regions to 26% in humid regions) and 18% (from 13% in dry regions to 39% in humid regions), respectively. The impact of the land surface initialization is fairly modest: the R^2 values range from 2% in dry regions to 8% in humid regions for P forecasts and from 6% in dry regions to 9% in humid regions for T_{sfc} forecasts.

Comparing the changes in signal-to-noise ratio and R^2 values (Figs. 5c and 5d, and 6c and 6f) shows that the regions where the potential predictability increases coincide largely with those where the signal-to-noise ratio increases. This is seen more easily in a scatterplot showing the relationship between the signal-to-noise ratio and R^2 changes due to the land surface initialization (Fig. 7). The positive relationship implies that the increased external variance forced by the land surface conditions is transferred to potential predictability.

The geographical dependence found in the signal-to-noise ratio and R^2 values might depend on the local strength of the land–atmosphere interaction. The evaporation efficiency (E/R_{net}, where E is the total evaporation and R_{net} is the total incident radiation) can be considered as a regional indicator of the strength of the land–atmosphere interaction, as it characterizes the capability of the modeling system to realize available soil moisture into the atmosphere by the evaporation process. Figure 8 categorizes the increases in R^2 values in Fig. 6 by evaporation efficiency for all global grid points. For the P forecasts, large increases in R^2 are mostly observed in the evaporation efficiency range of 0.4–0.7 (i.e., over humid regions, as indicated by the blue color), whereas only modest increases are observed in intermediate and dry regions. With the current modeling system, higher evaporation rates generally imply larger predictability for P forecasts. For the

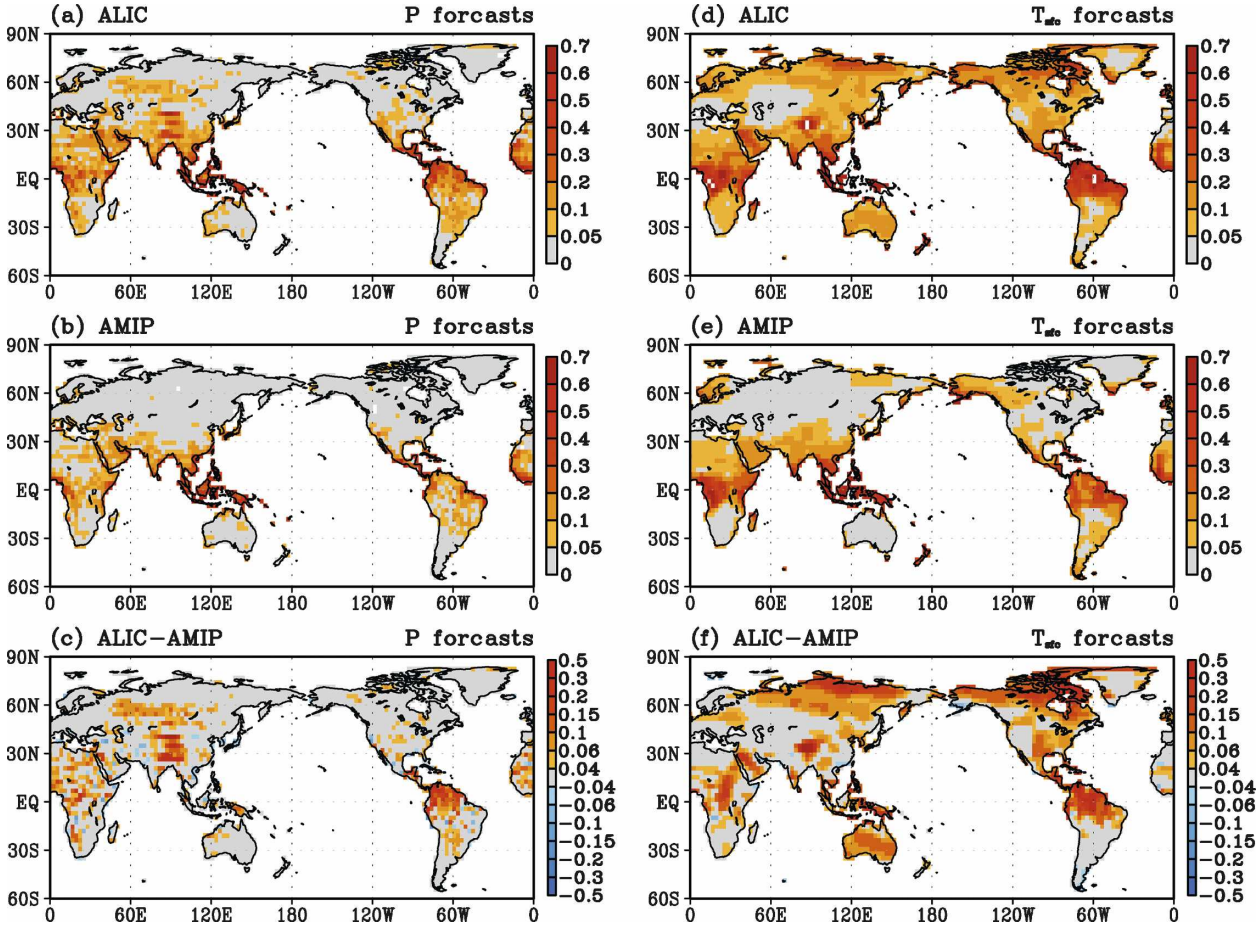

FIG. 6. The R^2 statistics for idealized forecasts for (a), (d) ALIC, (b), (e) AMIP, and (c), (f) its difference for (left) precipitation and (right) surface air temperature forecasts. Values of 0.04, 0.06, and 0.10 in (c), (f) are significant at the 90%, 95%, and 99% levels, respectively.

T_{sfc} forecasts, the increases in R^2 are generally larger than that for the P forecasts, and the largest increases are found in regions similar to those for the P forecasts. However, large increases are also observed in the low evaporation efficiency range of 0.1–0.3, maybe over northern Eurasia, North America near the Arctic region, and Australia. This signal seems to be due to the long persistence of the land surface conditions over these relatively dry, high-latitude regions, where variations in soil moisture and evaporation are very limited due to the very small amount of precipitation.

TABLE 4. Same as in Table 3, but for the R^2 statistic.

	Region	ALIC	AMIP	Difference
Precipitation	Humid	0.26	0.19	0.08 (40)
	Intermediate	0.10	0.06	0.03 (51)
	Dry	0.07	0.05	0.02 (45)
	Global	0.10	0.07	0.03 (45)
Surface air temperature	Humid	0.39	0.30	0.09 (29)
	Intermediate	0.19	0.12	0.07 (55)
	Dry	0.13	0.07	0.06 (76)
	Global	0.17	0.11	0.06 (55)

c. *Practical skill with respect to observation*

Up to now, the impacts of the land surface initialization have been discussed based on idealized predictability without any direct comparison between the ensemble simulations and observations. Now we examine the predictability through direct comparison between the forecasts and observations. Instead of the R^2 statistics, we used the signed explained variance $R^{*2} = r|r|$ (r is the correlation coefficient between the monthly averaged ensemble mean and the observations) suggested by Dirmeyer (2006). As the information concerning the sign is included, this method is appropriate for estimating the increase in practical predictability represented by the differences between the ALIC and

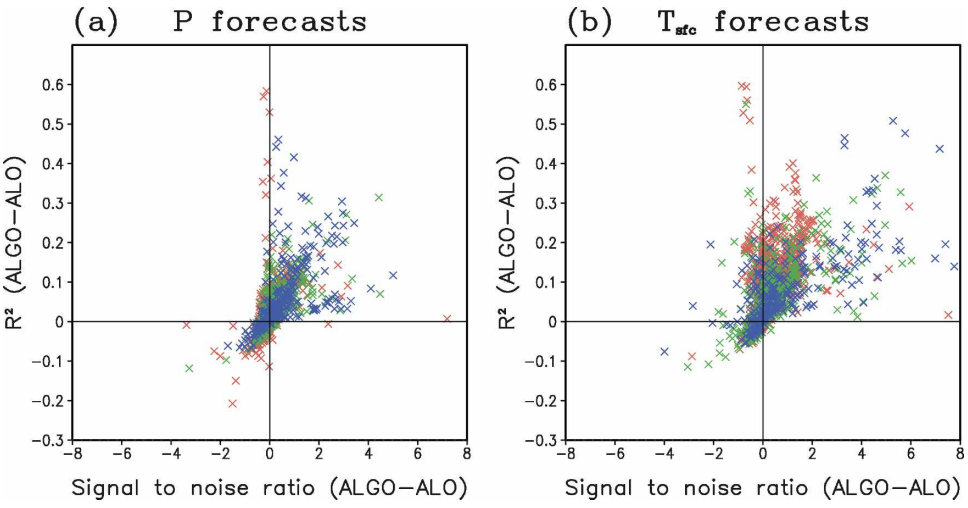

FIG. 7. Scatterplot for the R^2 differences between ALIC and AMIP: (a) precipitation and (b) surface temperature. The x axis represents the signal-to-noise difference between ALIC and AMIP. Blue, green, and red dots indicate humid, intermediate, and dry regions, respectively.

AMIP predictions. For the P and T_{sfc} forecasts, the R^{*2}_{ALIC} values are shown in Figs. 9a and 9b, and the predictability gains from land surface initialization (defined as $R^{*2}_{ALIC} - R^{*2}_{AMIP}/1 - R^{*2}_{AMIP}$) are shown in Figs. 9c and 9d. The normalizing denominator $1 - R^{*2}_{AMIP}$ is the unrealized predictability of the AMIP simulation, which varies from 0 to 2, so the predictability gain represents how much of the predictability is realized by land surface initialization. It should be noted that both the ALIC and the AMIP are simulated without an atmospheric initialization; therefore, the predictabilities are influenced by only the effects of the prescribed SSTs and land surface conditions.

Overall, the ALIC experiment explains only a very limited portion of the observed total variability. While most continental points represent modest positive R^{*2} values (approximately 10%), some negative values are also found. Relatively strong positive values are found in T_{sfc} forecasts, mostly over coastal regions, which are probably influenced by the adjacent oceans and the prescribed observed SSTs. The gains, ALIC minus AMIP, show localized features. Most of the positive

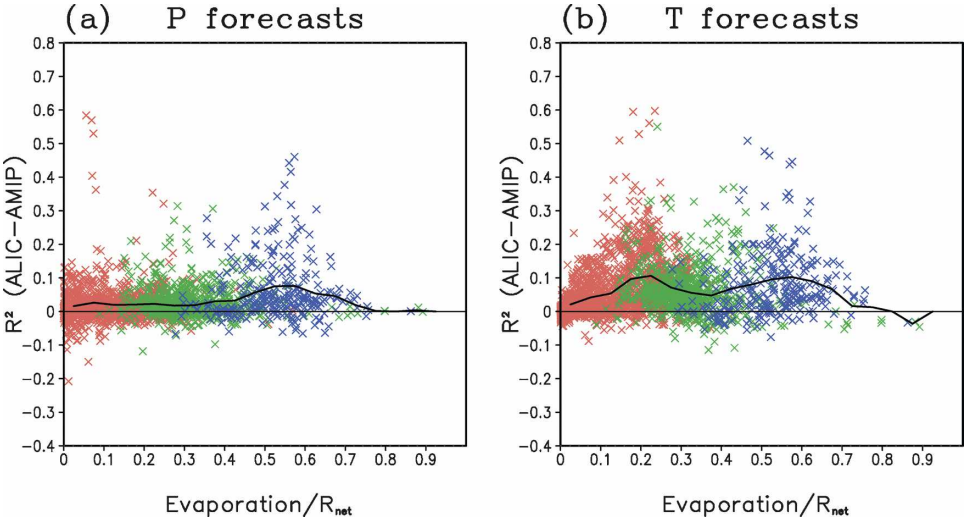

FIG. 8. As in Fig. 7, but here the x axis represents the evaporation efficiency The black solid line indicates the fitted curve of dots by use of a simple binning procedure with a 0.05 interval for the evaporation efficiency.

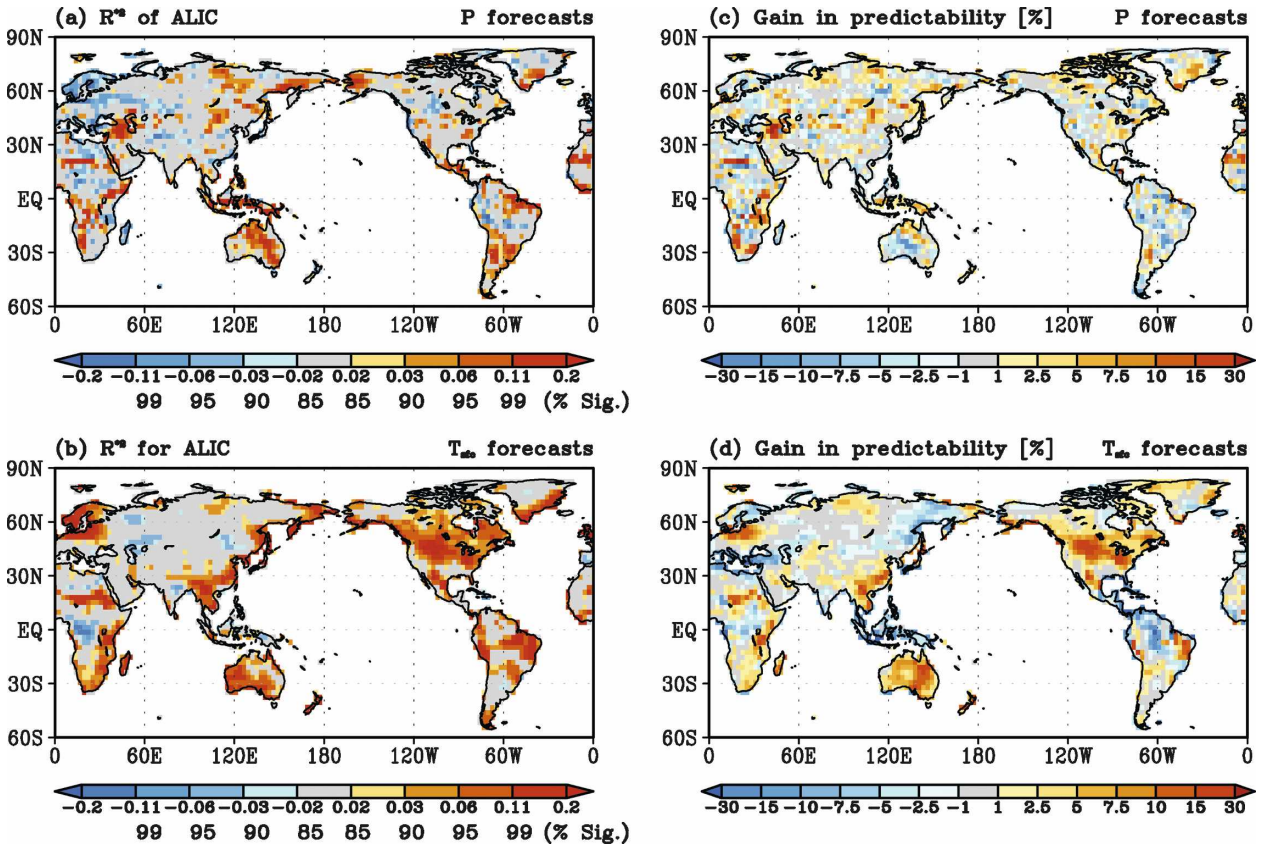

FIG. 9. (a), (b) The signed explained variance of ALIC and (c), (d) the gain in predictability of ALIC with respect to AMIP for (top) precipitation and (bottom) surface air temperature forecasts.

gains are observed over relatively dry and intermediate regions, such as middle Eurasia, middle to eastern North America, and mid- to southern Africa, which roughly matches the idealized predictability (Figs. 6c and 6f). This indicates the realization of idealized potential predictability over these regions. However, the gains are almost absent in humid regions, and negative gains (deteriorated predictability) are seen particularly for the Amazon and northeastern Eurasia. As Dirmeyer (2006) and Koster and Suarez (2003) suggested, the relatively high mean precipitation over these regions tends to quickly remove the initialized land surface memory (i.e., the atmospheric control on the land surface is dominant); therefore, the prescribed land surface conditions have less impact on predictability. Another fact to consider is that the density of the direct observations is very scarce over these regions of negative gains (see Fig. 2 in Koster et al. 2004a). Thus, the initialized land surface conditions would be biased with respect to the observations and cause negative effects on the proper simulation of subsequent land–atmosphere interactions. The inadequate station density might also affect the validation result in Fig. 6.

The 1-month forecast skill in ALIC relies mostly on the interannual variation of the GSWP2 forcings, which is memorized in initial land surface conditions used in the ensemble experiment. To examine the impact of interannual variation of land surface conditions, an additional CAM3 hindcast experiment, ALIC_CLIM, was performed and the calculated R^{*2} is presented in Fig. 10. Compared to the ALIC results in Fig. 9 (left panels), ALIC_CLIM shows very low R^{*2} predictability except over some tropical latitudes where the direct impact of SST is strong. Especially for T_{sfc}, most of the positive R^{*2} disappear when interannual variations are removed from land surface conditions. Although the gains from land surface initialization (as shown in Fig. 9) are modest, this last result shows that the predictability gains do indeed result from land surface initial conditions, and especially from the interannual variations.

4. Summary and discussion

In the present study, ensemble hindcast simulations of AGCM (CAM3) were performed both with and

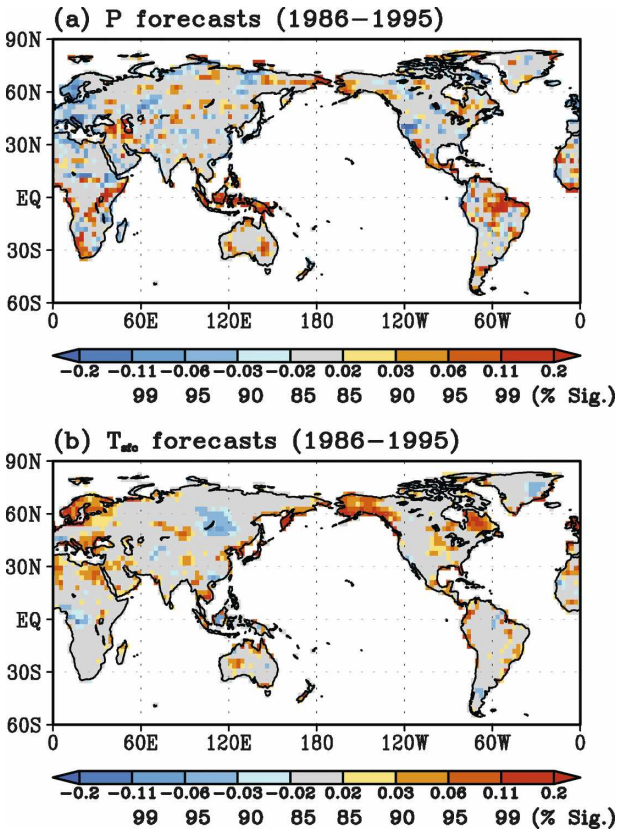

FIG. 10. Explained signed variance (R^{*2}) of the ALIC_CLIM simulation for (a) precipitation and (b) surface air temperature.

without land surface initialization from offline LSM (CLM3) calculations, and the impacts on predictability were examined. An alternative approach to initializing the land surface conditions was introduced. Prior to the offline LSM calculations, bias correction and anomaly scaling were applied to meteorological forcings that drive the offline LSM calculation. Statistical analyses on ensemble simulations indicated a modest but promising potential predictability increase from using this land surface initialization method. Even though there was no marked improvement in the practical predictability, our land surface initialization approach was shown to effectively estimate realistic land surface conditions that successfully provided land surface memory in the modeling system while preventing the AGCM climate drift problem. However, several limitations need to be considered and overcome to obtain any further enhancement in practical predictability.

First, the experimental design of this study might have led to some discrepancies between the land and atmosphere in the early stages of model integration, while in reality the land and atmosphere are tightly coupled. In drought situations, for example, the dry land surface is usually overlaid by a warm, dry atmosphere. This results in a simple land–atmosphere feedback process that can provide land-originated predictability: The dry soil condition results in less evaporation, which further induces less precipitation. However, no effort was made to ensure the initial atmospheric conditions were consistent with the initialized land surface conditions in the ALIC experiments. So, continuing the example, if the initial atmospheric conditions used produce significant precipitation in the early stages of forecasts, then any effects of the land surface initialization will soon disappear. Thus, enhanced predictability could be achieved in an AGCM simulation if the observed atmospheric initial conditions were incorporated, particularly by an assimilation system.

Second, in the present study the impacts of the land surface initialization are presented for the boreal summer simulation as a whole. However, the climatic properties that determine the strength of a land–atmosphere interaction possess considerable nonstationarity (i.e., seasonality), even within the summer; the impacts of land surface initialization inevitably reflect this nonstationarity. Such seasonal factors can be highly influential in monsoonal regions where distinct changes in precipitation, net radiation, and circulation regimes accompany the seasonal march of the monsoon. Figure 11 displays the monthly R^2 from May to September separately. Generally, the potential predictability and its change by land surface initialization show similar features to Fig. 6 (the entire summer), but possess distinct seasonality in some regions. Over the East Asian monsoonal region, both the R^2 and predictability gains are very small for the months of June and July when there is large monsoonal precipitation. In contrast, relatively high R^2 values and gains are maintained during the entire summer over northern South America, which is also a tropical region, but where the monsoonal variation is very weak. Over the central United States, which has been suggested by many previous studies as being a key region of strong land–atmosphere interaction, R^2 and gains for P were almost absent in the entire summer calculation (Fig. 6). However, although some positive gains were obtained in the monthly calculations, their locations vary greatly with month. The most distinct nonstationarity was found in the T_{sfc} forecasts over the Australian continent; gains gradually increase and reach a maximum in July, and then gradually decrease in August and September. More attention should be paid to seasonality should the experiments be conducted for winter, because snow dynamics would be involved in the hydrological cycle and land–atmosphere interaction. These considerations could provide a more

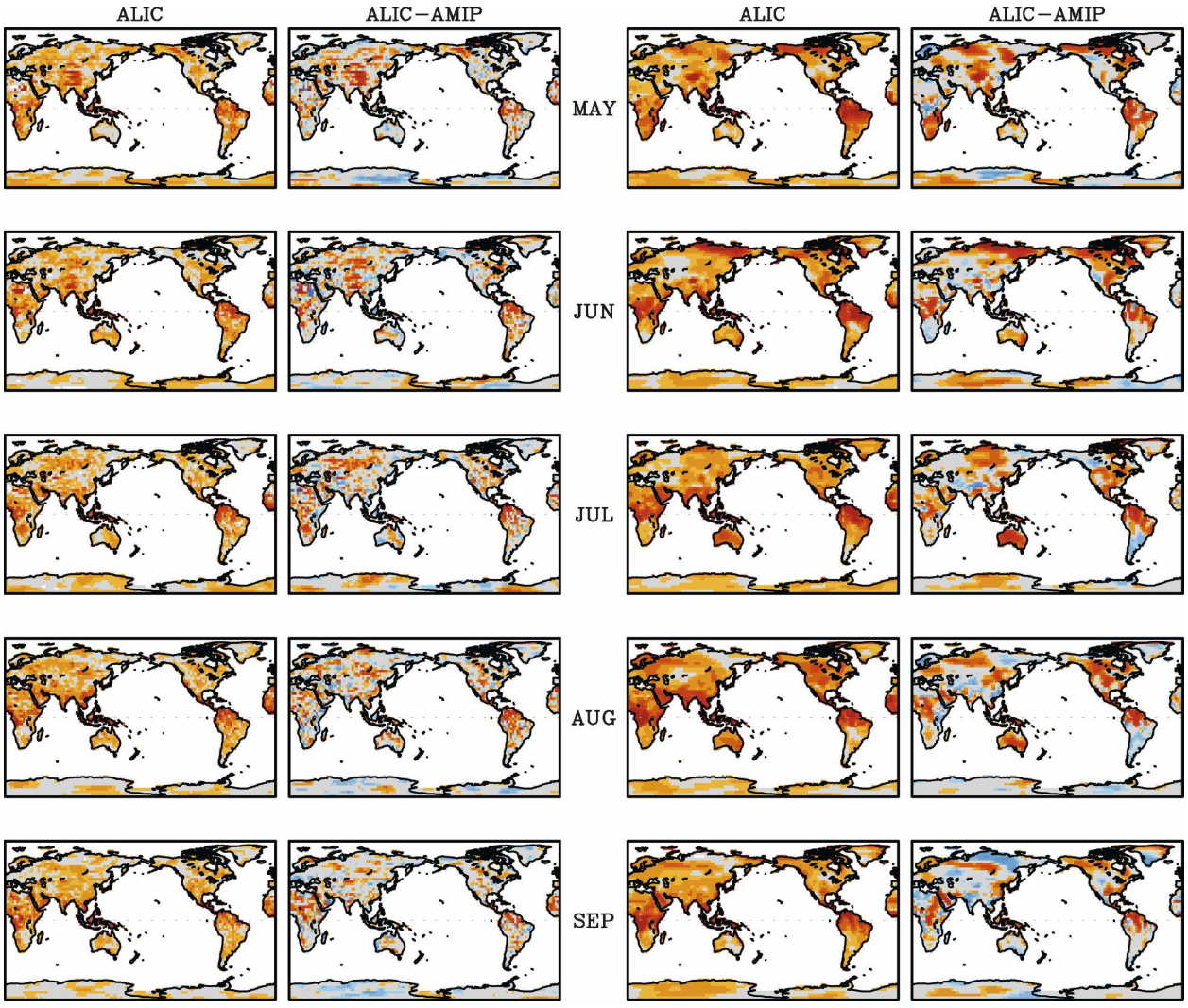

FIG. 11. The R^2 statistics for idealized forecasts for ALIC and their deviations from AMIP for each month (May–Sep) for (left) precipitation and (right) surface air temperature forecasts. Shading information is as in Fig. 6.

precise understanding of the land–atmosphere interaction and guide the predictability gains for seasonal prediction.

The present results are confined to the CAM3–CLM3 model; consequently, both the land surface estimates by the offline LSM and ensemble AGCM experiments are dependent on the inherent characteristics of CLM3 and CAM3, respectively. By virtue of the up-to-update dynamical and physical treatments incorporated, CAM3 is known to successfully simulate most of the climate variability realistically. Although substantial improvements have been achieved in recent decades, there are still great deficiencies in midlatitude continental precipitation and surface temperature (Collins et al. 2006), as shown in Fig. 1. As suggested by an offline LSM study by Mahanama and Koster (2005), such AGCM biases lead to a biased evaporative regime in certain regions and consequently have negative effects on soil moisture memory and land–atmosphere feedback. While the climate drift problem is eliminated by correcting the bias in atmospheric forcings to match the AGCM's individual climatology, the realism of the land–atmosphere interactions is still limited by the AGCM's individual bias. Thus, improving the model to reduce climate bias is the most essential factor for an appropriate simulation of land–atmosphere interactions and consequent predictability increases. Further, the efforts of multi-LSM-based land surface estimates like GSWP2 and their multi-AGCM evaluation through the Global Land–Atmosphere Coupling Experiment (GLACE; Koster et al. 2004b, 2006) can help reduce the uncertainties in single-model results. The

correction method suggested here could easily be applied to these efforts.

Acknowledgments. This study was funded by the Korea Meteorological Administration Research and Development Program under Grant CATER 2006-4204. David Rayner improved the English.

REFERENCES

Bonan, G. B., K. W. Oleson, M. Vertenstein, S. Levis, X. Zeng, Y. Dai, R. E. Dickinson, and Z.-L. Yang, 2002: The land surface climatology of the Community Land Model coupled to the NCAR Community Climate Model. *J. Climate,* **15,** 3123–3149.

Calvet, J.-C., J. Noilhan, J.-L. Roujean, P. Bessemoulin, M. Cabelguenne, A. Olioso, and J.-P. Wigneron, 1998: An interactive vegetation SVAT model tested against data from six contrasting sites. *Agric. For. Meteor.,* **92,** 73–95.

Collins, W. D., and Coauthors, 2004: Description of the NCAR Community Atmosphere Model (CAM 3.0). NCAR Tech. Note NCAR/TN-464+STR, Boulder, CO, 214 pp.

——, and Coauthors, 2006: The Community Climate System Model version 3 (CCSM3). *J. Climate,* **19,** 2122–2143.

Conil, S., H. Douville, and S. Tyteca, 2007: The relative influence of soil moisture and SST in climate predictability explored within ensembles of AMIP type experiments. *Climate Dyn.,* **28,** 125–145.

Dirmeyer, P. A., 2000: Using a global soil wetness dataset to improve seasonal climate simulation. *J. Climate,* **13,** 2900–2922.

——, 2001: Climate drift in a coupled land–atmosphere model. *J. Hydrometeor.,* **2,** 89–100.

——, 2006: The hydrologic feedback pathway for land–climate coupling. *J. Hydrometeor.,* **7,** 857–867.

——, Z. Guo, and X. Gao, 2004: Comparison, validation, and transferability of eight multiyear global soil wetness products. *J. Hydrometeor.,* **5,** 1011–1033.

——, X. Gao, M. Zhao, Z. Guo, T. Oki, and N. Hanasaki, 2006: The Second Global Soil Wetness Project (GSWP-2): Multimodel analysis and implications for our perception of the land surface. *Bull. Amer. Meteor. Soc.,* **87,** 1381–1397.

Entin, J. K., A. Robock, K. Y. Vinnikov, S. E. Hollinger, S. Liu, and A. Namkhai, 2000: Temporal and spatial scales of observed soil moisture variations in the extratropics. *J. Geophys. Res.,* **105,** 11 865–11 877.

Gates, W. L., and Coauthors, 1999: An overview of the results of the Atmospheric Model Intercomparison Project (AMIP I). *Bull. Amer. Meteor. Soc.,* **80,** 29–55.

Hirabayashi, Y., T. Oki, S. Kanae, and K. Musiake, 2003: Application of satellite-based surface soil moisture data to simulating seasonal precipitation. *J. Hydrometeor.,* **4,** 929–943.

International GEWEX Project Office, 2002: GSWP-2: The second global soil wetness project science and implementation plan. IGPO Publication Series, No. 37, 65 pp.

Kanae, S., Y. Hirabayashi, T. Yamada, and T. Oki, 2006: Influence of "realistic" land surface wetness on predictability of seasonal precipitation in boreal summer. *J. Climate,* **19,** 1450–1460.

Kang, I.-S., and J. Shukla, 2006: Dynamic seasonal prediction and predictability of the monsoon. *The Asian Monsoon,* B. Wang, Ed., Springer, 585–612

Koster, R. D., and M. J. Suarez, 2003: Impact of land surface initialization on seasonal precipitation and temperature prediction. *J. Hydrometeor.,* **4,** 408–423.

——, ——, and M. Heiser, 2000: Variance and predictability of precipitation at seasonal-to-interannual timescales. *J. Hydrometeor.,* **1,** 26–46.

——, and Coauthors, 2004a: Realistic initialization of land surface states: Impacts on subseasonal forecast skill. *J. Hydrometeor.,* **5,** 1049–1063.

——, and Coauthors, 2004b: Regions of strong coupling between soil moisture and precipitation. *Science,* **305,** 1138–1140.

——, and Coauthors, 2006: GLACE: The Global Land–Atmosphere Coupling Experiment. Part I: Overview. *J. Hydrometeor.,* **7,** 590–612.

Liu, Y., and R. Avissar, 1999: A study of persistence in the land–atmosphere system with a fourth-order analytical model. *J. Climate,* **12,** 2154–2168.

Mahanama, S. P. P., and R. D. Koster, 2005: AGCM biases in evaporation regime: Impacts on soil moisture memory and land–atmosphere feedback. *J. Hydrometeor.,* **6,** 656–669.

Oki, T., S. Seto, and K. Musiake, 2000: Land surface monitoring by backscattering from TRMM/PR 2A21. *Proc. Int. Geoscience and Remote Sensing Symp.,* Honolulu, HI, IEEE, 2032–2034.

Oleson, K. W., and Coauthors, 2004: Technical description of the Community Land Model (CLM). NCAR Tech. Note NCAR/TN-461+STR, Boulder, CO, 174 pp.

Reynolds, R. W., and T. M. Smith, 1994: Improved global sea surface temperature analyses using optimum interpolation. *J. Climate,* **7,** 929–948.

Robock, A., K. Y. Vinnikov, G. Sirinivasan, J. K. Entin, S. E. Hollinger, N. A. Speranskaya, S. Liu, and A. Namkhai, 2000: The Global Soil Moisture Data Bank. *Bull. Amer. Meteor. Soc.,* **81,** 1281–1299.

Rowell, D. P., 1998: Assessing potential seasonal predictability with an ensemble of multidecadal GCM simulations. *J. Climate,* **11,** 109–120.

Shukla, J., 1981: Dynamical predictability of monthly means. *J. Atmos. Sci.,* **38,** 2547–2572.

Vinnikov, K. Ya., A. Robock, N. A. Speranskaya, and A. Scholosser, 1996: Scales of temporal and spatial variability of midlatitude soil moisture. *J. Geophys. Res.,* **101,** 7163–7174.

Wagner, W., G. Lemoine, and H. Rott, 1999: A method for estimating soil moisture from ERS scatterometer and soil data. *Remote Sens. Environ.,* **70,** 191–207.

Wu, W., and R. E. Dickinson, 2004: Time scales of layered soil moisture memory in the context of land–atmosphere interaction. *J. Climate,* **17,** 2752–2764.

Zhao, M., and P. A. Dirmeyer, 2003: Production and analysis of GSWP-2 near-surface meteorology data sets. COLA Tech. Rep. 159, Center for Land–Ocean–Atmosphere Studies, Calverton, MD, 38 pp.